

Microfluidics of cytoplasmic streaming and its implications for intracellular transport

Raymond E. Goldstein^{*†‡}, Idan Tuval^{*}, and Jan-Willem van de Meent^{*§}

^{*}Department of Applied Mathematics and Theoretical Physics and [†]Cambridge Computational Biology Institute, University of Cambridge, Wilberforce Road, Cambridge CB3 0WA, United Kingdom; and [§]Instituut-Lorentz/Leiden Institute of Physics, Universiteit Leiden, Postbus 9506, 2300 RA, Leiden, The Netherlands

Edited by Robert H. Austin, Princeton University, Princeton, NJ, and approved January 2, 2008 (received for review August 1, 2007)

Found in many large eukaryotic cells, particularly in plants, cytoplasmic streaming is the circulation of their contents driven by fluid entrainment from particles carried by molecular motors at the cell periphery. In the more than two centuries since its discovery, streaming has frequently been conjectured to aid in transport and mixing of molecular species in the cytoplasm and, by implication, in cellular homeostasis, yet no theoretical analysis has been presented to quantify these processes. We show by a solution to the coupled dynamics of fluid flow and diffusion appropriate to the archetypal “rotational streaming” of algal species such as *Chara* and *Nitella* that internal mixing and the transient dynamical response to changing external conditions can indeed be enhanced by streaming, but to an extent that depends strongly on the pitch of the helical flow. The possibility that this may have a developmental consequence is illustrated by the coincidence of the exponential growth phase of *Nitella* and the point of maximum enhancement of those processes.

advection–diffusion | algae | cyclosis | *Chara* | metabolism

Since Bonaventura Corti’s discovery (1) in 1774 of the persistent circulation of the cytoplasm of plant cells, the phenomenon now known as cytoplasmic streaming or cyclosis has been conjectured to play an important role in metabolism (2). It occurs in organisms as diverse as amoebae (3), algae and terrestrial plants (4, 5), and fungi (6). In plants (4, 5, 7) it is driven by multitudes of the motor protein myosin moving along bundled actin at the boundary of the cytoplasm, carrying microscopic particles or organelles (8, 9), and entraining fluid. The motion of protoplasmic granules entrained in the flow includes unidirectional streaming, “fountain streaming” (in which the motion near the central axis of the cell is opposite to that near the periphery), and spiral “rotational streaming.”

Plant myosins can move at tens of micrometers per second (10–13), considerably faster than most animal myosins (although some can reach $\approx 30 \mu\text{m/s}$), and the speed U of cyclosis can reach $\approx 100 \mu\text{m/s}$ in cells whose radius R can reach 0.5 mm. These speeds greatly outpace diffusion, as measured by the Péclet number $Pe = UR/D$, where D is a molecular diffusion constant. For the smallest molecules, with $D \sim 10^{-5} \text{ cm}^2/\text{s}$, we see that $Pe \sim 50$, and it can easily reach 500–1,000 for larger proteins. The fact that transport by fluid motion becomes necessary to outrun the slow pace of diffusion in larger organisms, as emphasized in the celebrated essay by Haldane on size in biology (14), has been a theme in discussions of cytoplasmic streaming for many years. Yet, there has been little theoretical work and fewer experiments that have quantified the full implications of cytoplasmic streaming for transport and mixing. Only recently has it been recognized (2, 15) that the large Péclet numbers found *in vivo* could enhance metabolite exchange with organelles such as chloroplasts. Still, a range of basic questions has remained unanswered (16): What is the role of cytoplasmic streaming in homeostasis? How does streaming affect metabolic rates? Why has nature chosen the often complex flow geometries seen in plants?

Here, we propose answers to these questions by examining the most basic aspects of streaming flows, motivated by the phe-

nomenology of *Chara corallina* (Fig. 1), which historically has been an organism of choice for studies of streaming (4). We develop the simplest hydrodynamic model of the rotational streaming flow of *Chara* and *Nitella*, and demonstrate very strong enhancement of mixing within the cell and of nutrient uptake from the environment, both correlated directly with the helical geometry of flow. Such flows constitute a previously uncharacterized solution found by evolution to transport on the microscale, complementary to the great variety of mechanisms proposed to enhance mixing in microfluidic devices (17).

Background

Chara corallina is an algal weed inhabiting ponds, consisting of a slender stem interrupted by nodes, from each of which sprout several branches. The cylindrical branches that connect the nodes are exceptionally large single cells 1 mm in diameter and up to 10 cm long (Fig. 1). These multinucleated “internodal” cells have chloroplasts along the inside of the cell wall, arranged in rows that are organized in a helical manner. The surface of the cell is divided into two helical bands with wavelength $\lambda \sim 1 \text{ cm}$. These two domains are separated by two “indifferent zones,” which can be identified by missing rows of chloroplasts and are visible as a pair of diametrically opposite light lines spiralling along the internodal cell. Bundles of actin filaments line the inside of the chloroplast rows. Filamentary actin is a polar polymer, and its orientation determines the direction of motion of myosin. The two spiralling bands have opposite polarity, resulting in upward streaming along one band and downward streaming along the other. The result is aptly called the “barber pole” flow (Fig. 2), and the indifferent zones are therefore regions of high shear. Actin is localized in the cytoplasm, a region some 10–20 μm thick that is separated from the larger interior vacuole by the tonoplast, a membrane within which is a complex set of ion channels and pumps that tightly control numerous metabolic functions by keeping the cytosolic concentrations of ions and metabolites optimal, by storing nutrients, and by dynamically responding to external environmental conditions (18–20).

There is a hierarchy of questions one can ask about the fluid dynamics of streaming: the force–velocity relationship of individual motor proteins [a well studied problem (13)], the collective dynamics of interacting motors (21), the generation of shear by motors ferrying cargo, and ultimately the large-scale flow driven by that shear at the cell wall. Some aspects of the latter problem in fluid dynamics were studied long ago (22), with attention restricted to the radial velocity profile at a given cross-section, and for nonspiralling flows (23).

Author contributions: R.E.G., I.T., and J.-W.v.d.M. designed research; R.E.G., I.T., and J.-W.v.d.M. performed research; I.T. and J.-W.v.d.M. analyzed data; and R.E.G., I.T., and J.-W.v.d.M. wrote the paper.

The authors declare no conflict of interest.

This article is a PNAS Direct Submission.

[†]To whom correspondence should be addressed. E-mail: r.e.goldstein@damtp.cam.ac.uk.

© 2008 by The National Academy of Sciences of the USA

F1,AQ:C

AQ: D

APPLIED PHYSICAL SCIENCES

BIOPHYSICS

F2

AQ: I

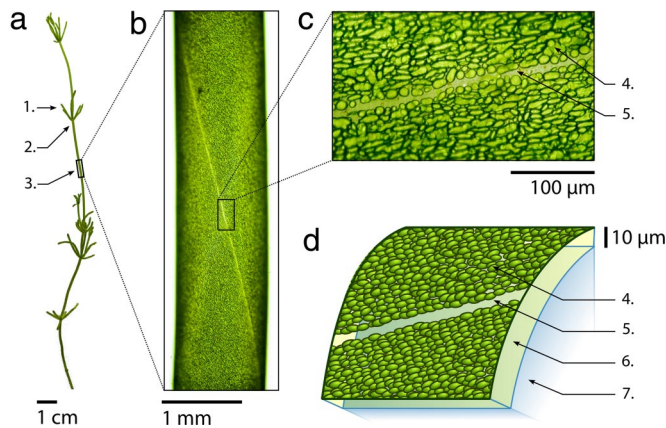


Fig. 1. Architecture of *Chara corallina*. (a) Portion of a plant, with leaf cells (1), nodes (2), and internodal cells (3). (b) Enlargement of an internodal cell, displaying spiraling indifferent zone. (c) Close-up of the indifferent zone. (d) Schematic cross-section: chloroplasts (4), indifferent zone (5), endoplasm (6), and vacuole (7).

In considering large-scale transport, it is important to note that motion in the vacuole may well be important. Although the actively sheared layer of cytoplasm encompasses $<10\%$ of the cellular volume, experiments dating back to the pioneering work of Kamiya and Kuroda (7) show that motion in the cytoplasm drives flow throughout the vacuole. Moreover, those flows are consistent with complete transmission of stress through the tonoplast (23). The mechanism by which this motion is transmitted has yet to be elucidated by quantitative studies. Lipid membranes do behave as two-dimensional fluids and can support shear (24). There is also evidence for continual production of moving ripples in the tonoplast, seen by light microscopy and with fluorescently labeled tonoplasts (25, 26), and these could influence the shear transmission.

In addition to a possible role in gravitational sensing (27), several scenarios have been put forward recently to explain the role of cyclosis in metabolism (2, 16), focusing on the possible consequences of longitudinal (node to node) transport. Although likely

crucial for intercellular communication, it is important to reiterate that metabolism in the multinucleated internodal cells differs from that in higher organisms, where the sources of nutrients and metabolites are far from the loci of energy production and consumption. Within the characean internodal cells it would appear that there is no general need to transport things longitudinally from place to place because all three processes occur ubiquitously within the cytoplasm along the whole cell length. Instead, the very act of moving cytoplasmic fluid past the fixed chloroplasts may increase their rate of exchange of molecular species with that fluid (15). However, can streaming enhance the mixing of cellular contents? If the fluid motion were strictly longitudinal in the cytoplasm, the dominant contribution to mixing in the thin cytoplasmic layer would take place at the indifferent zones and would be very inefficient on the scale of the entire cell. Given the tight biochemical linkage that the tonoplast creates between the vacuolar fluid and the cytoplasm, examination of mixing flows in the vacuole then becomes of great importance.

Results and Discussion

Because our interest here is the implication of spiraling flow on molecular transport, we take as a given the transmission of shear across the tonoplast and consider flow and transport in a cylindrical cell, given spiral forcing at the wall. Note that in this approach, fine details of the velocity within the cytoplasm and in the neighborhood of the tonoplast (22) are not resolved. The mathematical problem we consider is the coupled partial differential equations for the low Reynolds number fluid velocity \mathbf{u} of the incompressible vacuolar fluid ($\nabla \cdot \mathbf{u} = 0$),

$$\eta \nabla^2 \mathbf{u} = \nabla p, \quad [1]$$

and the advection-diffusion dynamics for a concentration C of a nutrient or metabolite,

$$C_t + \mathbf{u} \cdot \nabla C = D \nabla^2 C. \quad [2]$$

Here, p is the pressure and η is the fluid viscosity. The exterior of the cell will be taken to be a saturated reservoir of the metabolite concentration C . At the cell wall are velocities of $\pm U$ along the spiral directions. Prescribed forces there may also be considered and lead to quantitatively similar results. The solu-

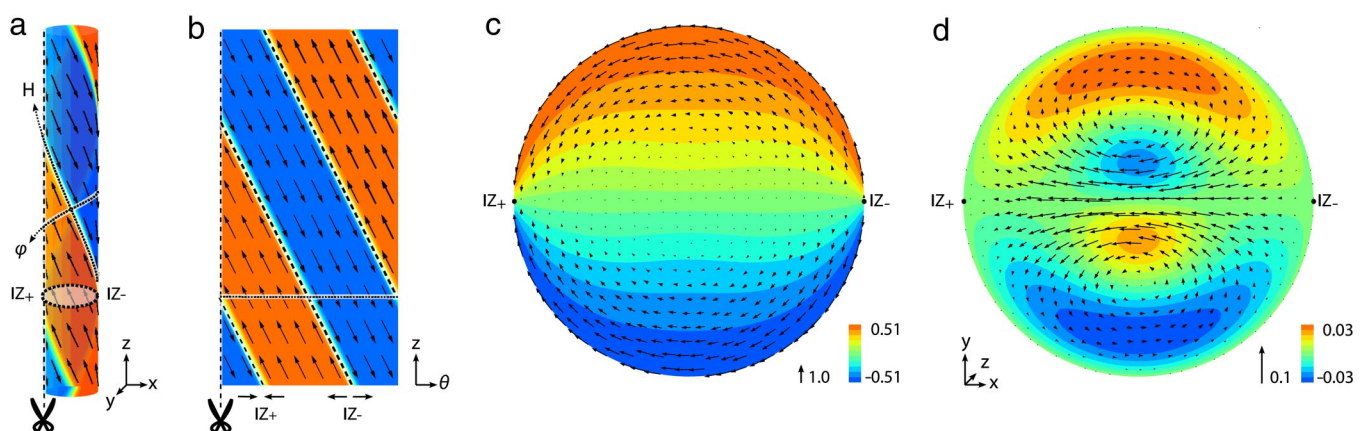


Fig. 2. Idealized spiraling flow in *Chara*. (a) Flow at the boundary, divided in an ascending band (red) and descending band (blue) separated by two indifferent zones (yellow, labeled $IZ_{+/-}$). Vectors indicate the direction of flow along the bands. Arrows labeled H and ϕ indicate the axes parallel and perpendicular to the spiral. The shaded region corresponds to the horizontal section shown by its intersection with the boundary as a horizontal solid line in b and viewed along the cell axis in c and d . (b) Cylinder from a , cut open along dotted line (as indicated by scissors) and flattened out. Ascending and descending regions now appear as diagonal bands. The two indifferent zones have a subtle difference in symmetry, which is reflected in the horizontal components of motion converging at one zone and diverging for the other, as indicated by the arrows at bottom. (c) Projection of the flow along the spiraling axis (with z axis into page), for a cross-section marked by the circle in a , with $\lambda/R = 3$. Contours and arrows denote the z - and xy - components of $v(r, \phi)H$, respectively. (d) Velocity field components orthogonal to H , denoted by $J(r, \phi)$. This transversal flow is smaller than the spiraling component by an order of magnitude and is zero at the wall, where flow is parallel to the spiral.

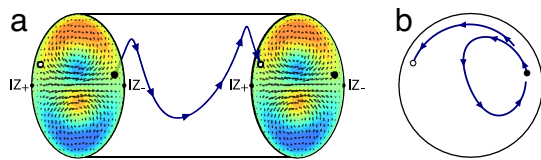


Fig. 3. Spiralling flow. (a) Trajectory of a fluid parcel over one cycle of longitudinal transport for $\lambda/R = 3$. (b) Projection of the trajectory onto the xy -plane.

tion of Eqs. 1 and 2 is simplified by exploiting the helical symmetry of the flow. Because internodal cells can reach 10 spirals in length, we neglect the effect of cell ends (28) and study an infinite cylinder with wavelength λ . Previous work on flows with helical symmetry (29, 30) shows that the solution decomposes into two terms,

$$\mathbf{u} = v(r, \varphi) \mathbf{H} + \mathbf{J}(r, \varphi), \quad [3]$$

where the first is the component parallel to the spiral and the second is perpendicular to the spiral and in the radial direction.[¶]

The helical properties of the flow produce qualitatively different advection–diffusion dynamics than the nonspiraling case. In a cell with straight indifferent zones (helical wavelength $\lambda \rightarrow \infty$), the vector \mathbf{H} in Eq. 3 is parallel to \hat{z} , a unit vector along the cell axis, and the transverse component $\mathbf{J} = 0$; the flow is purely longitudinal within each half-cylinder. This case reduces to the solution found by Pickard for the flow in a nonspiraling cell (23). If the concentration outside of the cell has cylindrical symmetry, then the concentration C inside of the cell will also have that symmetry. Thus, the vector ∇C points only in the radial direction, which is perpendicular to the fluid velocity field \mathbf{u} , so $\mathbf{u} \cdot \nabla C$ is identically zero; transverse advection plays no role in the dynamics even though the Péclet number is formally large.

In the case of an internodal cell with finite pitch, the component \mathbf{J} introduces a fundamental asymmetry between the two indifferent zones that is determined by the chirality of the spiral. Fig. 2b shows a cylinder unwrapped into a strip, where the indifferent zones appear as parallel diagonal bands at an angle $\alpha = \tan^{-1}(\lambda/2\pi R)$. Even without a detailed solution of the model, inspection of the flow vectors near the indifferent zones shows that the transverse (i.e., in-plane) components of the velocity are directed away from each other at one zone (IZ_-), whereas they converge at the other (IZ_+). The net effect is that there is in-plane flow from the region of IZ_- to the region of IZ_+ (hence the notation “–” for “into the cell center,” and “+” for “out from the cell center”). This component of the flow is completely negligible within cytoplasmic distances from the cell wall, ensuring that, at the resolution of the model, no fluid volumes cross the tonoplast. Nevertheless, we show in what follows the profound consequences these somewhat counterintuitive features, which have not been recognized previously, have on diffusive transport of the concentration C across the membrane. Fig. 2c and d shows a solution of the model through a mode expansion (31) (see *Materials and Methods*). These panels show the helical (left) and transverse (right) components of flow for a section at $z = 0$. The contours show the projection along the z axis of each of the velocities, with the vectors denoting its components in the xy plane. The transverse component \mathbf{J} takes the form of a weak spiraling circulation, whose magnitude is 1–5% of the bulk advection parallel to the indifferent zones.

The superposition of an in-plane circulation and the overall helical flow leads to intriguing three-dimensional trajectories of fluid particles. Fig. 3 shows a trajectory over one cycle of longitu-

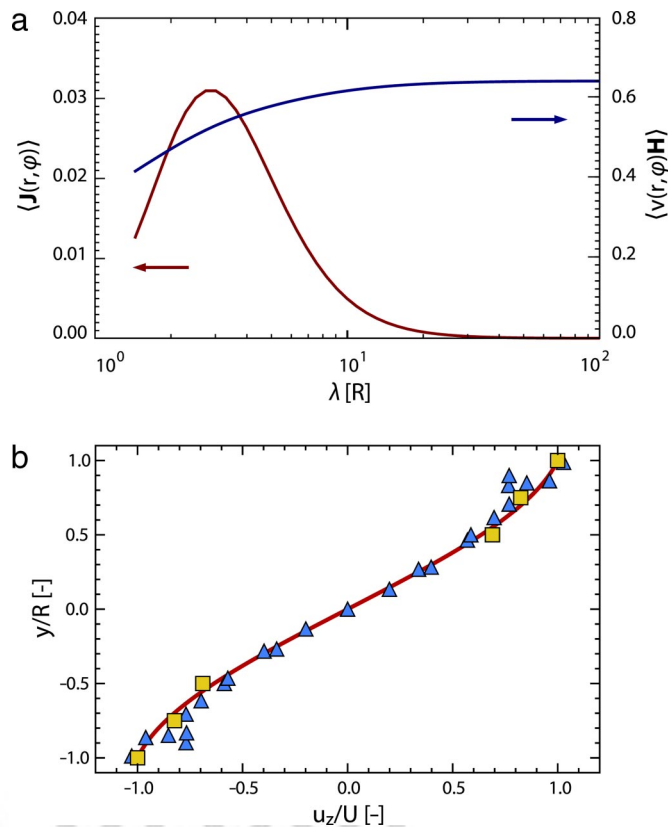


Fig. 4. Wavelength dependence and comparison with experiments. (a) Root-mean-square longitudinal (blue) and transversal (red) velocities as functions of helical wavelength. (b) Comparison of solved velocity to experimental data extracted from Kamiya and Kuroda (7) (yellow squares) and Mustacich (32) (blue triangles), where the velocities have been normalized to their maximum values, at the cell surface.

dinal transport, both in a lateral view and projected onto the xy plane. To illustrate the mixing dynamics, the initial position of the parcel was chosen near IZ_- : after one wavelength it has actually passed the opposite indifferent zone, IZ_+ . Thus, the combined effect of the spiraling and the longitudinal components of the flow is significant net movement of material across the vacuole.

The relative scales of the two flows vary with helical wavelength (Fig. 4a), the transverse component having a distinct maximum at $\lambda/R \approx 3$. The decline from this peak at large λ reflects the approach to purely longitudinal flow, whereas that at small λ/R arises from the cancellation of nearby opposing flows. By an argument analogous to the one given above for the vanishing of advective contributions for a cell with straight indifferent zones, the advective contribution from the helical component vanishes, but that from \mathbf{J} does not. It follows from the typical scale of \mathbf{J} that this contribution becomes important for Péclet numbers in excess of 10–100, as is the case in nature. The model also agrees well with existing data (7, 32) for the longitudinal velocity as a function of radius (Fig. 4b). Calculations for cylinders with closed ends indicate that the extent of the cross-flow is increased relative to the infinite cells (unpublished data).

Advection–diffusion dynamics in the regime of large Pe are generally associated with the formation of thin regions of high concentration gradients (“boundary layers”) near surfaces with vanishing fluid velocities, as in heat transport from solid spheres (33) or those with specified fluid velocities (34) or forces (35). Streaming dynamics are somewhat similar to these problems, but for exchange with the environment there is no steady-state with nonuniform concentration inside the cell unless there are internal

[¶]In the fluid dynamics literature, the second term in Eq. 3 is usually written as $\mathbf{J}(r, \varphi) = \mathbf{H} \times \nabla \Psi(r, \varphi)$, where Ψ is a helical generalization of the stream function.

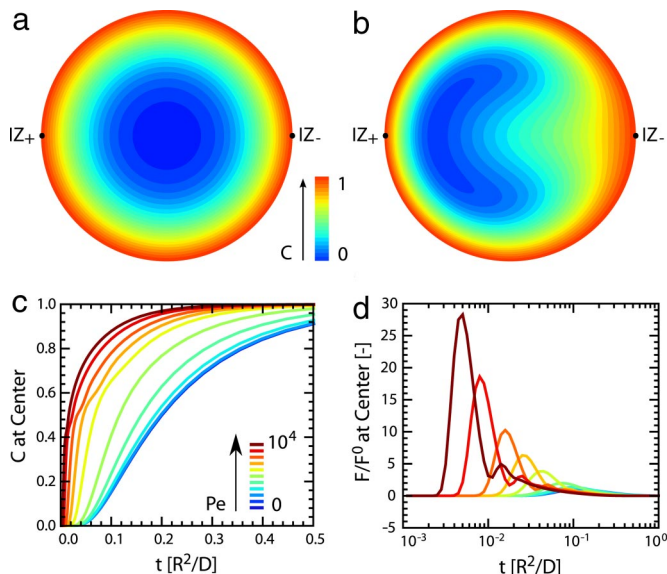


Fig. 5. Time-dependence of concentration during diffusion into cell. (a) In a cell with straight indifferent zones the concentration in a cross-section is azimuthally symmetric. (b) With a finite pitch ($\lambda/R = 3$) and $Pe = 500$ advection through the center of the cell (Fig. 2d) redistributes material, resulting in a steep concentration gradient at the left indifferent zone, which leads to a significant increase in the flux across the boundary. (c and d) Concentration at the center of the cell (c) and flux into a small cylinder at the center (d), for a series of Péclet numbers 10, 20, 50, ..., 10^4 . Low Péclet numbers are colored blue, and high Péclet numbers are colored red. Diffusion into the cell is significantly enhanced for high Pe .

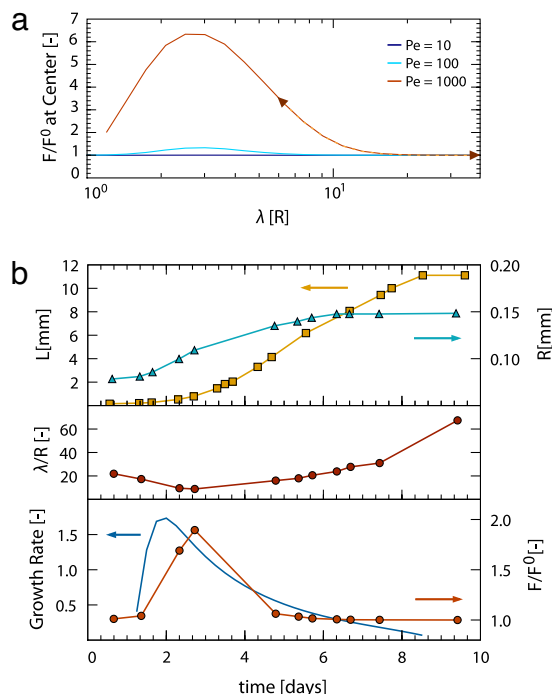


Fig. 6. Wavelength variations. (a) Flux enhancement at the center of a cell with constant concentration boundary conditions at the cell wall as a function of helix wavelength, at various Pe . (b) Comparison of calculated flux with data on growth of *Nitella axillaris* Braun, from Green (36). Blue triangles, cell diameter; orange squares, cell length; orange circles, helical wavelength in units of the cell radius. The flux enhancement (orange circles) at the cell center is calculated from model with rotational streaming and the nondimensionalized surface growth rate $S^{-1}dS/dt$ (blue solid curve), where S is the total surface area, calculated from spline-interpolated diameter and length. Arrowheads in a show the trajectory of wavelength over time, first decreasing and then increasing.

processes such as degradative chemical reactions that act as sinks. Here, we show that the transient dynamics can reflect the enhanced transport, and these are shown in Fig. 5. First, for a finite pitch, the transient displays an asymmetric concentration distribution due to advection by the transverse flow (Fig. 5b relative to a). This effect is quantified by the time evolution of the concentration at the cell center, and as the flux across a small circle near the cylinder center, for a range of Pe (Fig. 5c and d). We see a much more rapid rise of the center concentration and hence the flux at larger Pe . These shorter response times are essential for a fast dynamic adaptation to a changing environment and, therefore, for maintenance of homeostasis. There are, additionally, scaling laws for the time and magnitude of the flux maximum that reflect the tendency toward boundary-layer formation mentioned above (unpublished data). Intriguingly, for sufficiently large Pe , the thickness of the region of highest concentration gradients can be comparable to the width of the cytoplasm.

Flow-enhanced rates of exchange with the environment depend strongly on the helical wavelength. Clearly, decreasing the pitch will decrease the transport flux from one end of a cell to the other. If longitudinal transport were the only purpose to streaming, a cell with straight indifferent zones is optimal. However, as shown in Fig. 6a, the maximum of the advection-enhanced flux of C into the cell depends on the wavelength in a manner similar to the radial velocity shown in Fig. 4a. For the observed range of values, the inward flux generally follows the opposite tendency to the longitudinal flux, suggesting an optimization process at work.

The dependence of transport on helical pitch may have implications for cellular growth. Green (36) made detailed measurements of the changing geometry in *Nitella axillaris* Braun cells as they grow by following marker particles attached to the exterior cell surface. Fig. 6b is a replotted of those results for the cell length, radius, and helical wavelength. We see that during early development the spiral wavelength decreases to a minimum that coincides with the maximum relative elemental growth rate.

Our model calculations show that this wavelength/radius ratio is also a maximum in the nutrient uptake rate from the environment. It is then a plausible conjecture that nature has chosen helical flows to enhance the uptake rate, particularly at this significant developmental stage.

The model calculations also show that there is strong heterogeneity in the uptake rate over the cell surface. The greatest contribution from advection occurs in the neighborhood of the indifferent zones, and because the flows near the two zones are different, so too is the flux across them. This can be seen in Fig. 7, where we show the flux normalized to that in the absence of flow for the case $\lambda/R = 12$ and for various Péclet numbers. The difference in uptake rate

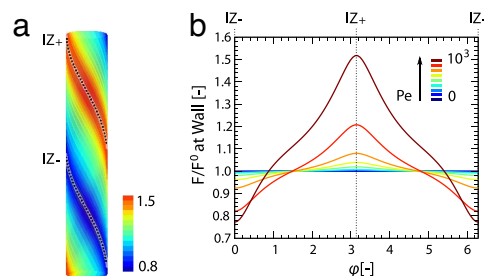


Fig. 7. Heterogeneity in the uptake rate of a cell for $\lambda/R = 12$. (a) Color-coded rate of uptake on the cell surface, for $Pe = 1,000$. (b) Enhancement of flux through a circular region near the cell wall due to fluid flow for various values of the Péclet number (0, 10, 20, 50, ..., 10^3), as a function of azimuthal angle.

between the maximum and minimum can be as large as the mean value.

Conclusions

The analysis presented here immediately suggests a number of specific experimental investigations. Chief among them are detailed studies of the geometry of flow, using appropriate tracer particles, to examine the asymmetry between the indifferent zones and their importance in mixing. The predicted variations in uptake rate across the cell surface suggest the possibility that photosynthetic activity itself might be spatially varying around the periphery of the organism. This can be tested with fluorescence methods (37) used in the study of photosynthetic activity in leaves. In such an investigation, it would be important to separate out the effects of variations in chloroplast size and intrinsic activity from effects of nutrient exchange. Finally, the connection between helical streaming in internodal cells and the fast circulatory streaming in the nodes remains to be elucidated. Taken together with recent work (35, 38) on the dynamics of advection by flagellated multicellular algae (e.g., *Volvox*), and collective flows in concentrated bacterial suspensions (39), the present analysis serves to highlight the unusual features of “life at high Péclet numbers,” in which advection dominates diffusion.

Materials and Methods

Stokes flow was solved as a mode expansion in cylindrical coordinates (31). Adopting a radial coordinate rescaled by the cell radius, the velocity field takes the form

$$\begin{aligned} u_r(r, \varphi) &= \sum_{n \text{ odd}} u_r^n(r) \cos(n\varphi) \\ u_\theta(r, \varphi) &= \sum_{n \text{ odd}} u_\theta^n(r) \sin(n\varphi) \\ u_z(r, \varphi) &= \sum_{n \text{ odd}} u_z^n(r) \sin(n\varphi) \\ p(r, \varphi) &= \sum_{n \text{ odd}} p^n(r) \cos(n\varphi). \end{aligned} \quad [4]$$

We impose the velocity $\tilde{u}(1, \phi)$ at the boundary. The radial component $u_r(1, \phi) = 0$ and the remaining two components are decomposed into Fourier modes.

The radial modes are most readily solved by the substitutions $u_r^n = -(a^n + b^n)/2$ and $u_\theta^n = -(a^n - b^n)/2$, after which one finds simple combinations of modified Bessel functions:

$$\begin{aligned} a_r^n(r) &= \frac{1}{I_n(n\kappa)} \left[A^n I_{n+1}(n\kappa r) + P^n \frac{\kappa r}{2\pi} I'_{n+1}(n\kappa r) \right] \\ b_r^n(r) &= \frac{1}{I_n(n\kappa)} \left[B^n I_{n-1}(n\kappa r) + P^n \frac{\kappa r}{2\pi} I'_{n-1}(n\kappa r) \right] \\ u_z^n(r) &= -\frac{1}{I_n(n\kappa)} \left[E^n I_n(n\kappa r) + P^n \frac{\kappa r}{2\pi} I'_n(n\kappa r) \right] \\ p_r^n(r) &= -\frac{1}{I_n(n\kappa)} \left[P^n \frac{\kappa}{\pi} I_n(n\kappa r) \right]. \end{aligned} \quad [5]$$

The pressure coefficients may now be eliminated using the incompressibility condition, which reduces to $P^n = -n\pi(A^n + B^n - 2E^n)$. Substitution of $r = 1$ into the above yields a linear system of equations, from which A^n , B^n , and E^n can be determined in terms of the Fourier decomposition of $\tilde{u}(1, \varphi)$. Computations used a smooth transition across the indifferent zone, with a width of $\pi/16$.

Numerical solution of the advection diffusion equation was done by substitution of helically symmetric modes for the concentration:

$$C(r, t) = \sum_n C^n(r, t) \cos(n\varphi). \quad [6]$$

The ODEs for the temporal evolution of the radial modes are discretized in r and integrated by using the Fortran-based LSODE solver (40), with 24 density modes, each with 100 radial grid points.

ACKNOWLEDGMENTS. We are deeply indebted to Prof. Dina F. Mandoli for introducing us to this problem and for ongoing collaborations and to Prof. Nina S. Allen for numerous discussions on the mechanism of streaming. We also thank J. Banfield, M. Croft, J. Davies, J. Haseloff, J. O. Kessler, E. Macrobie, J. Mestel, T. J. Pedley, and especially W. van Saarloos for important discussions. This work was supported by the Human Frontier Science Program (I.T.), the Engineering and Physical Sciences Research Council (J.-W.v.d.M.), the University of Leiden (J.-W.v.d.M.), Department of Energy Grant DE-AC02-06CH11357, and the Schlumberger Chair Fund (R.E.G.).

AQ: G

- Corti B (1774) *Osservazione Microscopiche sulla Tremella e sulla Circolazione del Fluido in Una Planto Acquaguola* (Appresso Giuseppe Rocchi, Lucca, Italy).
- Pickard WF (2003) *Plant Cell Environ* 26:1–15.
- Allen RD, Allen NS (1978) *Annu Rev Biophys Bioeng* 7:469–495.
- Shimmen T (2007) *J Plant Res* 120:31–43.
- Allen NS, Allen RD (1978) *Annu Rev Biophys Bioeng* 7:497–526.
- Cole L, Orlovich DA, Ashford AE (1998) *Fungal Genet Biol* 24:86–100.
- Kamiya N, Kuroda K (1956) *Bot Mag Tokyo* 69:544–554.
- Kachar B (1985) *Science* 227:1355–1357.
- Kachar B, Reese TS (1988) *J Cell Biol* 106:1545–1552.
- Chaen S, Inoue J, Sugi H (1995) *J Exp Biol* 198:1021–1027.
- Yamamoto K, Hamada S, Kashiyama T (1999) *Cell Mol Life Sci* 56:227–232.
- Sugi H, Chaen S (2003) *J Exp Biol* 206:1971–1976.
- Shimmen T, Yokota E (2004) *Curr Opin Cell Biol* 16:68–72.
- Haldane JBS (1985) *On the Importance of Being the Right Size* (Oxford Univ Press, Oxford).
- Pickard WF (2006) *J Theor Biol* 240:288–301.
- Hochachka PW (1999) *Proc Natl Acad Sci USA* 96:12233–12239.
- Squires TM, Quake SR (2005) *Rev Mod Phys* 77:977–1026.
- Reisen D, Marty F, Leborgne-Castel N (2005) *BMC Plant Biol* 5:13.
- Wink M (1993) *J Exp Bot* 44:231–246.
- Martinoia E, Maeshima M, Neuhaus HE (2007) *J Exp Bot* 58:83–102.
- Houtman D, Pagonabarraga I, Lowe CP, Esseling-Ozdoba A, Emons AMC, Eiser E (2007) *Europhys Lett* 78:18001.
- Nothnagel EA, Webb WW (1982) *J Cell Biol* 94:444–454.
- Pickard WF (1972) *Can J Bot* 50:703–711.
- Noguchi H, Gompper G (2004) *Phys Rev Lett* 93:258102.

- Cutler SR, Ehrhardt DW, Griffiths JS, Somerville CR (2000) *Proc Natl Acad Sci USA* 97:3718–3723.
- Yoneda A, Kutsuna N, Higaki T, Oda Y, Sano T, Hasezawa S (2007) *Protoplasma* 230:129–139.
- Staves MP (1997) *Planta* 203:S79–S84.
- Pickard WF (1974) *Protoplasma* 82:321–339.
- Zabieliski L, Mestel AJ (1998) *J Fluid Mech* 370:297–320.
- Childress S, Landman M, Strauss H (1989) in *Proceedings of the IUTAM Symposium on Topological Fluid Mechanics*, eds Moffatt HK, Tsinober A (Cambridge Univ Press, Cambridge, UK), pp 216–224.
- Meleshko VV, Malyuga VS, Gomilko AM (2000) *Proc R Soc London Ser A* 456:1741–1758.
- Mustacich RV, Ware BR (1977) *Biophys J* 17:229–241.
- Acrivos A, Taylor TD (1962) *Phys Fluids* 5:387–394.
- Magar V, Goto T, Pedley TJ (2003) *Q J Mech Appl Math* 56:65–91.
- Short MB, Solari CA, Ganguly S, Powers TR, Kessler JO, Goldstein RE (2006) *Proc Natl Acad Sci USA* 103:8315–8319.
- Green PB (1954) *Am J Bot* 41:403–409.
- Daley PF, Raschke K, Ball JT, Berry JA (1989) *Plant Physiol* 90:1233–1238.
- Solari CA, Ganguly S, Kessler JO, Michod RE, Goldstein RE (2006) *Proc Natl Acad Sci USA* 103:1353–1358.
- Dombrowski C, Cisneros L, Chatkaew S, Kessler JO, Goldstein RE (2004) *Phys Rev Lett* 93:098103.
- Hindmarsh AC (1983) in *HIMACS Transactions on Scientific Computation*, eds Stepleman RS, Carver M, Peskin R, Ames WF, Vichnesvetsky R (North-Holland, Amsterdam), Vol 1, pp 55–64.

APPLIED PHYSICAL
SCIENCES

BIOPHYSICS

AQ: H